processes

MDPI

Article

Techno-Economic Assessment of PEM Electrolysis for O_2 Supply in Activated Sludge Systems—A Simulation Study Based on the BSM2 Wastewater Treatment Plant

Mario Alejandro Parra Ramirez [1], Stefan Fogel [1], Sebastian Felix Reinecke [1,*] and Uwe Hampel [1,2]

[1] Institute of Fluid Dynamics, Helmholtz-Zentrum Dresden-Rossendorf, 01328 Dresden, Germany; m.parra-ramirez@hzdr.de (M.A.P.R.); s.fogel@hzdr.de (S.F.); u.hampel@hzdr.de (U.H.)
[2] Chair of Imaging Techniques in Energy and Process Engineering, Technical University of Dresden, 01062 Dresden, Germany
* Correspondence: s.reinecke@hzdr.de

Abstract: The conversion of renewable energy into hydrogen (H_2) by power-to-gas technologies involving electrolysis is seen today as a key element in the transition to a sustainable energy sector. Wastewater treatment plants (WWTP) could be integrated into future green H_2 networks as users of oxygen (O_2) produced alongside H_2 in water electrolysis. In WWTPs, O_2 is required for biological treatment steps, e.g., in activated sludge (AS) systems. However, the production costs of electrolysis O_2 should be competitive with those of conventional O_2 production processes. In this study, mathematical models of a polymer electrolyte membrane electrolyser (PEME) plant and the WWTP of the Benchmark Simulation Model No. 2 (BSM2) were used to simulate electrolysis O_2 supply to an AS system and estimate net costs of production (NCP) for produced O_2 via a techno-economic assessment (TEA). Assuming that produced H_2 is sold to a nearby industry, NCPs for O_2 were calculated for two different PEME plant dimensions, four alternatives regarding electricity supply and costs, and three sets of assumptions regarding system performance and market conditions. The analyses were performed for 2020 as a reference year and 2030 based on forecasts of relevant data. Results of the dimensioning of the PEME show the O_2 demand of a municipal WWTP with an installed capacity of 80,000 population equivalents (PE), such as the one of the BSM2, can be covered for more than 99% of the simulated period by either a 6.4 MW PEME operated for 4073 full load hours or a 4.8 MW PEME operated for 6259 full load hours. Investment costs for the PEME stacks and the operational costs for electricity make up most of the NCP of electrolysis O_2. The projected decrease in PEME stack costs and renewable energy prices in favourable market conditions can result in a competitive NCP for electrolysis O_2 in 2030. The approach described in this study can be applied to analyse O_2 supply to biological wastewater treatment in WWTPs with different characteristics, in processes different from AS, and under different assumptions regarding economic conditions.

Keywords: wastewater treatment; activated sludge; PEM electrolysis; techno-economic assessment

Citation: Parra Ramirez, M.A.; Fogel, S.; Reinecke, S.F.; Hampel, U. Techno-Economic Assessment of PEM Electrolysis for O_2 Supply in Activated Sludge Systems—A Simulation Study Based on the BSM2 Wastewater Treatment Plant. *Processes* **2023**, *11*, 1639. https://doi.org/10.3390/pr11061639

Academic Editors: Dimitris Zagklis and Georgios Bampos

Received: 22 March 2023
Revised: 22 May 2023
Accepted: 24 May 2023
Published: 26 May 2023

1. Introduction

The installed capacity of renewable energy sources has continued to increase at an ever-faster pace over the last few decades, promoted by growing concerns regarding the effects of climate change and technological improvements in wind and photovoltaic (PV) power generation systems. However, as the share of weather-dependent, variable renewable energy sources in the energy mix continues to increase, new approaches for grid management become necessary to cope with fluctuating energy availability and ensure a stable and safe supply [1]. Power-to-gas technologies in which electrical renewable energy is converted into green hydrogen (H_2) via electrolysis are considered a key process in the energy grid of the future with applications in transport, chemical, and industrial processes, as well as for long-term energy storage and management [2–4]. Until recently, one of

the main barriers to the industrial-scale production of green H_2 was the high cost of the electrolyser stacks. Nevertheless, if the current trends of decreasing renewable energy costs and improvements in electrolyser technologies continue in the future, green H_2 will have the potential to become a competitive and sustainable alternative to fossil H_2 in large-scale applications [3,5,6].

Wastewater treatment plants (WWTPs) stand out among other industrial facilities for potential synergies with renewable based energy networks [7]. Their widespread location, the open areas usually available at their sites, and the expertise of personnel in the use of technical gases are among the advantages that WWTP offers for the installation of electrolyser systems [8]. From the WWTP site, produced H_2 can then be valorised internally as fuel, injected into the natural gas network, or supplied to industrial consumers nearby. H_2 can also be converted to methane by taking advantage of the carbon dioxide (CO_2) produced in the anaerobic digestion of sludge as a carbon source. This allows for the use of the biogas infrastructure available at WWTPs and existing natural gas networks [9,10]. Michailos et al. [10] have performed a techno-economic assessment (TEA) of five scenarios for biological methanation of electrolysis H_2 together with biogas coming from an anaerobic digester in a WWTP. The analysed scenarios differed in type of electrolyser, biological methanation process, and source of electricity. They concluded that, given a continuous trend of reduced costs for electrolysers and renewable power in the coming years, the produced methane could achieve lower levelized costs of energy (LCOE) than conventional natural gas.

Apart from the potential for H_2 use and storage, WWTP offers the possibility of exploiting produced oxygen (O_2) instead of discarding it into the atmosphere as a by-product. O_2 is required in WWTPs by microorganisms in biological treatment steps and can also be transformed into ozone (O_3) to be used for disinfection, micropollutant removal, and/or sludge conditioning through ozonation [7,8]. Gretzschel et al. [11] have carried out a feasibility study on the use of O_3 produced from electrolysis O_2 for micropollutant removal at a WWTP in Mainz, Germany. There, surplus energy coming from an on-site PV plant is used to operate a 1.25 MW alkaline water electrolyser to supply the 465,206 $kg \cdot a^{-1}$ of O_2 needed for the ozonation process. The authors concluded that savings of 47,000 $€ \cdot a^{-1}$ could be achieved by using electrolysis O_2 instead of buying liquid O_2 from an external provider. Regarding the use of pure O_2 for biological wastewater treatment, Skouteris et al. [12] have carried out a literature review on the effects of the use of pure O_2 on microorganism metabolism and pollutant removal. A higher treatment rate, reduced excess sludge, and better control of filamentous bacteria are presented as advantages reported for pure O_2, while lower pH in the mixed liquor and more refractory effluents are mentioned as possible disadvantages. With the aim of comparing the O_2 transfer process with air and pure O_2 in AS, Mohammadpour et al. [13] presented a mathematical model for bubble rising velocity and volumetric O_2 transfer coefficient ($k_L a$) depending on bubble size. The model is used to calculate the O_2 transfer rate (OTR) and transfer efficiency (OTE) for single bubbles of air and pure O_2 in clean water. Their results show an increase in OTE of approx. 10% for pure O_2 fine bubbles with respect to air injected at a 4 m water depth for conventional AS tanks, which leads to energy savings given by a lower required gas flowrate.

Industrial O_2 production costs have been sufficiently high so far to limit the number of WWTPs using pure O_2 for biological treatment, mainly those in locations with access to cheap O_2 from nearby producers or those requiring a higher OTR to treat heavily polluted and/or saline wastewater [12,14]. However, cost reductions associated with electrolysers and the respective increase in the installed capacity for green H_2 and O_2 production may lead to more favourable conditions for the use of electrolysis O_2 at WWTPs.

In the present study, mathematical models have been used to estimate the dimensions and costs of an electrolyser plant capable of covering the O_2 demand of a conventional AS system in a municipal WWTP and carry out an analysis of the economics of such a project under varying design, operational, and boundary conditions. The results obtained with the models are used together with reference values for economic parameters, namely prices of

pieces of equipment, supplies, electricity from conventional and renewable energy sources, H_2, and O_2, as the basis for a TEA on different scenarios.

2. Materials and Methods

2.1. Modelled System and Simulation Process

The modelled system consists of two sub-systems, namely a WWTP with a conventional AS system and a polymer electrolyte membrane electrolyser (PEME) plant installed at the WWTP site. PEME electrolysis was chosen for this study because, although the investment costs of PEMEs are currently higher than those for alkaline electrolysers, the first have shorter response times [15,16] and are therefore better qualified for green H_2 production with volatile a renewable energy supply. The PEME plant consists of sub-models for the PEME stack itself and its associated components, namely an AC/DC converter, a compressor, an intermediate gaseous O_2 storage tank, and a contingency liquid O_2 storage tank. Figure 1 shows a graphical representation of the modelled system. Further components, i.e., the PEME cooling system and water recirculation, are outside the scope of this study.

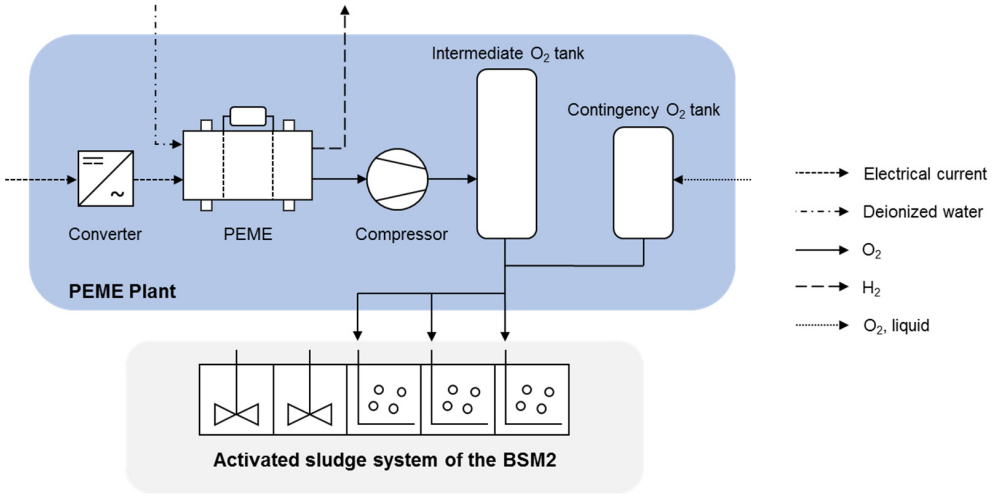

Figure 1. Graphical representation of the modelled system.

The electrolysis O_2 produced by the PEME is pressurized by the compressor and supplied to the intermediate storage tank before being injected into the AS tanks of the WWTP. The O_2 in the contingency storage tank is to be used when the intermediate storage is empty and the flowrate coming from the PEME is insufficient to cover the demand of the AS system. Produced H_2 is assumed to be directly supplied to an industrial site located near the PEME plant; therefore, H_2 storage tanks are not included in the system. The models were implemented into the SIMBA3 software tool developed by the Institute for Automation and Communication in Magdeburg, Germany [17]. All simulations were performed for one year of operation using a 15-min time step. The following sections describe the individual mathematical models for each of the subsystems.

2.2. WWTP Model Implementation and Estimation of O_2 Demand

The conceptual WWTP of the Benchmark Simulation Model No. 2 (BSM2) developed by the International Water Association (IWA) is used as a reference in this investigation. The BSM plant has an installed capacity of 80,000 population equivalents (PE) and includes primary settling, the AS system, secondary settling, and sludge treatment steps. The biological removal of nitrogen and carbon from wastewater is modelled using the Activated Sludge Model No. 1 (ASM1), a widely used mathematical model for the biochemical processes in AS systems, including oxygen demand, nitrification, and denitrification. The AS system of the BSM2 consists of five perfectly mixed tanks connected in series: two tanks for anaerobic denitrification and three tanks for aerobic nitrification. A complete description of the BSM2 plant and simulation procedure, as well as an overview of the ASM1, can be

found in [18]. The operation of the WWTP is simulated by using the dynamic influent file described in [19] as an input. This influent file is based on models for household and industrial wastewater production regimes and integrates the impact of weather conditions, i.e., dry, rain, and stormy weather, and temporal variations such as changes in wastewater production during workdays vs. weekends or population dynamics during holiday periods. Water temperature variations are also included in the influent file, affecting O_2 solubility and model parameters for biological activity in the ASM1 [18].

The oxygenation process is modelled in the BSM2 as variations in k_La values in nitrification tanks. The IWA has defined a default control scheme for the oxygenation system of the BSM2, consisting of a closed-loop configuration with a proportional integral controller (PI) that regulates the dissolved O_2 (DO) in the second nitrification tank by manipulating the values of k_La in all three nitrification tanks. In this study, the O_2 demand is calculated for the BSM2 operating with the default control strategy, for which the DO set-point is 2 gr·m^{-3}. A full description of the default control strategy can be found in [18]. Starting from the k_La time series resulting from BSM2 simulations, the OTR at a given time step is calculated for each nitrification tank i as follows:

$$OTR_i = \frac{1}{\alpha} \cdot k_L a_i \cdot (DO_{sat} - DO_i) \cdot V_{AS,i} \quad (1)$$

where α is the alpha factor for the AS (here, taken as 0.6 based on values reported in literature for pure O_2 AS systems [20]), DO_i and DO_{sat} are the measured and saturation O_2 concentrations, respectively, and $V_{AS,i}$ is the volume of the nitrification tank. In the BSMs, DO_{sat} at 15 °C is defined as 8 gr·m^{-3}; its dependency on temperature is described by the van't Hoff equation [21]. Since this study assumes the use of a 100% O_2 gas stream rather than air, the BSM2 has been modified in a way that DO_{sat} at 15 °C is equal to around 38.1 gr·m^{-3}, which corresponds to the original 8 gr·m^{-3} divided by 21% O_2 content in air. Temperature dependence is assumed to be described in the same way as in the original BSM2.

The corresponding nominal molar flow into the liquid phase ($\dot{n}^{AS}_{O_2,nom}$) is then calculated as the sum of the OTR_i values for all three nitrification tanks:

$$\dot{n}^{AS}_{O_2,nom} = \frac{1}{M_{O_2}} \cdot \sum_{i=1}^{3} OTR_i \quad (2)$$

where M_{O_2} is the molar mass of O_2. In conventional AS systems, a large share of the O_2 injected through diffusers is not transferred into the liquid phase but rather flows through into the atmosphere as bubbles. These losses can be represented by including a factor for the OTE of the diffuser system. The actual or effective O_2 flowrate that needs to be injected into the AS tanks ($\dot{n}^{AS}_{O_2,eff}$) can be expressed as:

$$\dot{n}^{AS}_{O_2,eff} = \frac{1}{OTE} \cdot \dot{n}^{AS}_{O_2,nom} \quad (3)$$

The OTE is taken here as a constant with a value of 60% for a conventional AS system [13,22]. Temporal variations in the OTE due to the effects of fouling or temperature changes have not been considered in this study.

2.3. PEME Plant Model Implementation

The PEME plant model includes mathematical expressions for power consumption and mass balances of O_2, H_2, and deionized water. The PEME follows an operation cycle with a one-day period, alternating between full and minimal load. The number of hours at full load operation depends on the availability of electricity, which is location-dependent in the case of renewable sources. Two scenarios for the PEME plant operation and corresponding dimensions are analysed, where scenario 2 has a longer time in full load operation than

scenario 1 (see Table 1). The values selected for the duration of full load operation are within the range of the scenarios reviewed in [23] and are meant to represent average and optimal electricity availability. An interlock is implemented in both scenarios to avoid breaching defined maximum (p_{max} of 15 bar) and minimum (p_{min} of 1.5 bar) overpressures in the intermediate O_2 tank. If the pressure in the intermediate tank approaches the defined limits (values above 14 bar or below 2.5 bar), the PEME switches to minimal or full load operation regardless of the predefined cycle.

Table 1. Time at full load operation of the PEME plant for the analysed scenarios.

Scenario	Nominal % of Day at Full Load	Nominal Full Load Hours $t_{FLH,nom}$ ($h \cdot a^{-1}$)
1	40	3504
2	75	6750

The PEME stack is assumed to operate in a low-pressure range, and the produced gases are extracted at atmospheric pressure. At full load, the input current density J is assumed to be 2.0 $A \cdot cm^{-2}$, at a minimum of 0.4 $A \cdot cm^{-2}$. The PEME cells have a total active area a_c of 1250 cm^2. The power of the PEME (P_{PEME}) can then be calculated as:

$$P_{PEME} = J \cdot a_c \cdot \varphi_{EZ} \tag{4}$$

where φ_{EZ} is the voltage of the electrolyser cells, which in turn depends on the input current density. Values for φ_{EZ} of 1.9 V at full load and 1.6 V at minimum load have been selected based on the compilation of PEME polarization curves presented in [24].

Since the starting times of PEMEs are usually below 15 min [16,25], changes in stack temperature and their effect on polarization curves during the start-up are neglected in the simulations. The gas and water flowrates have been calculated following the approach proposed in [15]. The molar flowrates of O_2, H_2, and deionized water in the electrolysis process are modelled using Faraday's law:

$$\dot{n}^{EZ}_{O_2,nom} = \frac{n_c \cdot J \cdot a_c}{4 \cdot F} \cdot \eta_f \tag{5}$$

$$\dot{n}^{EZ}_{H_2,nom} = \frac{n_c \cdot J \cdot a_c}{2 \cdot F} \cdot \eta_f \tag{6}$$

$$\dot{n}^{EZ}_{H_2O} = 1.25 \cdot \frac{n_c \cdot J \cdot a_c}{2 \cdot F} \cdot \eta_f \tag{7}$$

where $\dot{n}^{EZ}_{O_2,nom}$, $\dot{n}^{EZ}_{H_2,nom}$, and $\dot{n}^{EZ}_{H_2O}$ are nominal produced O_2, nominal produced H_2, and consumed deionized water, respectively. Furthermore, n_c is the number of electrolytic cells connected in the series, F is Faradays constant, and η_f is the faradaic efficiency (above 99% for water electrolysis). The effective H_2 and O_2 molar flowrates supplied by the PEME are then calculated by introducing the efficiency factor η_p, taken here as a constant equal to 75%, to account for losses during drying and purification steps after the cells:

$$\dot{n}^{EZ}_{O_2,eff} = \dot{n}^{EZ}_{O_2,nom} \cdot \eta_p \tag{8}$$

$$\dot{n}^{EZ}_{H_2,eff} = \dot{n}^{EZ}_{H_2,nom} \cdot \eta_p \tag{9}$$

The intermediate storage tank and the compressor are modelled following the approach described in [26]. The change in pressure in the intermediate storage tank, assuming ideal gas behaviour, can be expressed as:

$$\frac{dp_{sto}}{dt} = \frac{T_{sto} \cdot R}{V_{sto}} \cdot \left(\dot{n}^{EZ}_{O_2,eff} - \dot{n}^{AS}_{O_2,eff} \right) \tag{10}$$

where p_{sto}, T_{sto}, and V_{sto} are the pressure, temperature, and volume of the tank. T_{sto} is ideally controlled at 25 °C. The flow of O_2 gas from the intermediate storage tank in the PEME plant to the AS system is assumed to show ideal behaviour, and no further components (e.g., operation of valves) have been considered. The power consumption of the compressor P_{comp}, assumed here to be a centrifugal compressor, can be expressed as Equation (11):

$$P_{comp} = \frac{\dot{n}^{EZ}_{O_2,eff}}{\eta_{comp}} \cdot \frac{\kappa \cdot R \cdot T_{PEME}}{\kappa - 1} \cdot \frac{p_{sto}^{\frac{\kappa-1}{\kappa}}}{p_{PEME}} \quad (11)$$

where η_{comp} is the compressor efficiency (63%), κ is the polytropic exponent (1.62), T_{PEME} is the temperature of the PEME (ideally controlled at 80 °C), and p_{PEME} is the pressure of the PEME, taken here as atmospheric pressure.

The behaviour of the contingency O_2 storage tank is not modelled. The required flowrate of external O_2 ($\dot{n}_{O_2,ext}$) is equal to the demand of the AS system during the periods where the pressure in the intermediate tank is below the defined limit p_{min}:

$$\dot{n}_{O_2,ext} = \begin{cases} p_{sto} > p_{min}, & 0 \\ p_{sto} \leq p_{min}, & \dot{n}^{AS}_{O_2,eff} \end{cases} \quad (12)$$

The required contingency storage volume (V_{cont}) is then calculated based on the integral of $\dot{n}_{O_2,ext}$ over the simulation period. In a similar way, the behaviour of the AC/DC converter (transients and efficiency) is not modelled, and its capacity is assumed to be equal to the full load power of the PEME stack.

2.4. Techno-Economic Assessment

The TEA performed in this study considers the installation and operation of the PEME plant at the site of the conceptual BSM2 WWTP. The goal of the TEA is to gain insights on the development of the economics for the use of electrolysis O_2 in AS systems. For this, estimates of the net cost of production (from here on, C_{NCP}) of electrolysis O_2 are retrieved for PEME plants dimensioned according to the scenarios described in Table 1 and operating under different economic conditions. The obtained C_{NCP} values are then compared with those corresponding to O_2 produced in conventional industrial processes (e.g., in cryogenic air separation units). The presented TEA focuses on the implementation of the PEME plant, which means that the costs related to modifications in the design and operation of the WWTP (e.g., modifications to gas injection systems in AS tanks) are outside the scope of this investigation.

2.4.1. Cost Estimation Framework

The cost estimation framework for chemical industries described in [27] has been used as a reference for the calculation of C_{NCP} in the present study. C_{NCP} are derived based on the apparent capital (C_{CAPEX}) and operational expenditures (C_{OPEX}) attributed to the system components and operation. Capital expenditures are calculated using the factorial method. As a first step, the investment costs of the main pieces of equipment or purchased equipment costs (C_{PEC}) are estimated. The C_{PEC} include the costs of all components of the PEME plant model. The costs for the PEME stack, AC/DC converter, and compressor (C_i) are calculated using the capacity method as described in Equation (13) [27]:

$$C_i = C_{i,base} \cdot \left(\frac{S_i}{S_{i,base}} \right)^{\delta_i} \cdot \left(\frac{CEPCI}{CEPCI_{base}} \right) \quad (13)$$

where $C_{i,base}$ is the reference cost for an equipment unit i with a size or capacity $S_{i,base}$, S_i is the actual size or capacity of the equipment to be purchased, and δ_i is a reference empirical scaling exponent. The second term in Equation (13) accounts for historical changes in component costs. The Chemical Engineering Plant Cost Index (CEPCI) [28] is used here for historical cost scaling. The $CEPCI_{base}$ is the value of the index for the year of publication

of $C_{i,base}$ and $CEPCI$ is the value for the year of estimation. The reference values used for $C_{i,base}$, $S_{i,base}$, and δ_i can be found in Table 2, together with the year of publication of $C_{i,base}$. The corresponding values for $CEPCI_{base}$ and $CEPCI$ can be consulted under [29].

Table 2. Data used for the cost estimation for PEME stacks, the AC/DC converters, and compressors following the capacity method.

Equipment Item	$C_{i,base}$ (€)	$S_{i,base}$ (kW)	δ_i (-)	Reference	Year of Publication
PEME stack	1000 [a]	1	1	[3,30]	2020
AC/DC converter	160	1	1	[31,32]	2012
Compressor	267,000	445	0.67	[32,33]	2012

[a] Varies according to the value of PEME stack costs C_{PEME} in cost inventory (see Section 2.4.2).

The costs for the intermediate and contingency O_2 storage tanks for the AS ($C_{T,i}$) are calculated using a component-specific capacity method expression as:

$$C_{T,i} = n_{T,i} \cdot \left(a_{T,i} + b_{T,i} \cdot S_{T,i}^{\delta_{T,i}} \right) \cdot \left(\frac{CEPCI}{CEPCI_{base}} \right) \quad (14)$$

where $n_{T,i}$ is the number of tanks required to cover the designed volume. The corresponding values for the factors $a_{T,i}$, $b_{T,i}$, $\delta_{T,i}$, and the tank capacity $S_{T,i}$ can be found in Table 3.

Table 3. Data used for the cost estimation of the O_2 tanks following the capacity method.

Equipment Item	$a_{T,i}$ ($)	$b_{T,i}$ ($·kg^{-1})	$S_{T,i}$ (kg)	$\delta_{T,i}$ (-)	Reference	Year of Publication
Intermediate O_2 tank	12,800	73	7800	0.85	[27,34]	2010
Contingency O_2 tank	17,400	79	900	0.85	[27,34]	2010

The total purchased equipment costs (C_{PEC}) are determined as follows:

$$C_{PEC} = \sum C_i + \sum C_{T,i} \quad (15)$$

The obtained C_{PEC} are used to estimate the remaining cost items of C_{CAPEX}. All involved C_{CAPEX} cost items are estimated using the factorial approach based on the so-called Lang factors ($f_{CAPEX,i}$), which can be represented as an example of the case of ISBL costs (C_{ISBL}) as follows:

$$C_{ISBL} = \underbrace{C_{PEC}}_{\substack{Cost\ basis \\ (C_{CAPEX,i})}} \sum_{i=1}^{n} f_{CAPEX,i} \quad (16)$$

Table 4 summarizes the employed Lang factors $f_{CAPEX,i}$ for all superordinate cost items (C_{ISBL}, C_{OSBL}, C_{CC}, C_{DE}, C_{WC} and C_{SE}) that have been used in this study. Depending on the respective superordinate cost item, the different cost basis $C_{CAPEX,i}$ may be employed. Taking into account that the PEME plant is supposed to be installed at the site of an existing WWTP, cost items related to civil engineering and yard improvement required when a project is to be developed at a completely new site (so-called green field site) are not considered here.

Table 4. Capital expenditure C_{CAPEX} estimation methodology via the factorial method and chosen cost items and Lang factors based on literature data taken from [27,34,35].

Superordinate Cost Item $\sum_i C_{CAPEX,i} \cdot f_{CAPEX,i}$	**CAPEX Cost Item Description** $C_{CAPEX,i} \cdot f_{CAPEX,i}$	**Cost Basis (€)** $C_{CAPEX,i}$	**Index** i	**Lang Factor** $f_{CAPEX,i}$
Inside battery limits (C_{ISBL})	Equipment purchase	C_{PEC}	1	1
	Equipment installation		2	0.3
	Piping (installed) (valves, fittings, pipes, supports, and labour)		3	0.3
	Instrumentation and controls (installation labour, auxiliary equipment)		4	0.3
	Electrical systems (installed) (wiring, lighting, transformation, and services)		5	0.1
Outside battery limits (C_{OSBL})	Additions to site infrastructure Water, air and electricity supply nodes Piping, storage, and distribution	C_{ISBL}	6	0.1
Contingency charges (C_{CC})	Compensation of cost estimates Price/currency fluctuations Contractor/labour disputes	$C_{ISBL} + C_{OSBL}$	7	0.2
Design and engineering (C_{DE})	Engineering and supervision	$C_{ISBL} + C_{OSBL}$	8	0.3
	Construction expenses		9	0.3
	Contractor fee		10	0.1
Working capital (C_{WC})	Feed/product/spare parts inventory Cash on hand	$C_{ISBL} + C_{OSBL}$	11	0.1
Start−up expenses (C_{SE})	General start-up expenses	$C_{ISBL} + C_{OSBL}$	12	0.05

After calculating all relevant cost items, the total capital expenditures C_{CAPEX} can be determined based on the so-called fixed capital investments C_{FCI}, which represent the entirety of investment costs attributed to the planning/designing, construction, and erection of the plant, and the working capital C_{WC} and start-up expenses C_{SE}, which account for the capital used to maintain the plant's operation over its lifetime.

$$C_{CAPEX} = \underbrace{C_{ISBL} + C_{OSBL} + C_{CC} + C_{DE}}_{=C_{FCI}} + C_{WC} + C_{SE} \tag{17}$$

The operational costs C_{OPEX} can be subdivided into variable costs of production C_{VCP}, fixed costs of production C_{FCP}, and by-product revenues R_{H_2} from the sale of H_2:

$$C_{OPEX} = C_{VCP} + C_{FCP} - R_{H_2} \tag{18}$$

C_{VCP} are operational costs directly related to the plant´s output and therefore change with the operation mode, e.g., full or minimal load. For the estimation of C_{VCP}, the expression in Equation (19) is used:

$$C_{VCP} = C_{H_2O} + C_{O_2,ext} + C_E + C_{R,PEME} \tag{19}$$

where C_{H_2O} are the costs of the consumed deionized water, $C_{O_2,ext}$ are the costs of consumed liquid O_2 from the contingency tank, C_E are the costs of electricity, and $C_{R,PEME}$ are the costs for the replacement of PEME stacks until the plants end of lifetime (EOL). The yearly consumption of deionized water, liquid O_2, and electricity is obtained from the simulation results and is assumed to be constant until plants reach EOL. The respective specific costs of deionized water c_{H_2O}, external liquid O_2 $c_{O_2,ext}$, and electricity c_E are described in detail in Section 2.4.2.

The cost of PEME stack replacement $C_{R,PEME}$ is calculated based on the stack lifetime, plant lifetime, and cumulative full load operating hours. It is assumed that stack costs for each replacement are comprised of 50% of the initial specific PEME stack capital costs, as only the cells are replaced and the periphery and housing remain intact and are still usable.

Contrary to C_{VCP}, fixed costs of production C_{FCP} are independent of the actual operation or output of the plant. For the calculation of C_{FCP}, a factorial estimation methodology has also been applied (see Table 5 and Equation (20)).

$$C_{FCP} = \underbrace{c_{OL} \cdot y_{PL}}_{=C_{OL}} + \underbrace{(C_{WC} + C_{SE}) \cdot i_d \cdot y_{PL}}_{\substack{Capital\ charges \\ on\ WC/SE\ loan}} + \sum_{i=1}^{6} C_{OPEX,i} \cdot f_{OPEX,i} \quad (20)$$

Table 5. Fixed costs of production C_{FCP} estimation methodology based on the factorial method and retrieved Lang factors from the literature according to [27].

Superordinate OPEX/FCP Cost Item $C_{OPEX,i} \cdot f_{OPEX,i}$	**Cost Basis (€)** $C_{OPEX,i}$	**Index** i	**Lang Factor** $f_{OPEX,i}$
Supervision (C_{SV})	C_{OL}	1	0.25
Direct salary overhead (C_{DSO}) (Non-salary costs: Health insurance and benefits)	$C_{OL} + C_{SV}$	2	0.4
Maintenance (C_{MT})	C_{ISBL}	3	0.03
Property taxes and insurance (C_{PTI})	C_{ISBL}	4	0.01
Rent of land (C_{ROL})	$C_{ISBL} + C_{OSBL}$	5	0.01
Environmental charges (C_{EV})	$C_{ISBL} + C_{OSBL}$	6	0.01

The total operating labour costs C_{OL} represent the costs for the personnel in charge of the plant and are calculated based on the specific operating labour costs c_{OL}, taken here as 60,000 €·a^{-1}, and the plant's lifetime y_{PL}. Capital charges included within C_{FCP} are attributed to the interest payments on the loan of working capital and start-up expenses, which are supposed to be entirely funded by debt. These capital charges are included within C_{FCP}, since the total working capital and total start-up expenses are recovered at the EOL of the plant, and hence the incurring interest payments must not be included in the estimation of C_{CAPEX} via Equations (15) and (16) and Table 4 [27]. In Equation (20), i_d is the interest rate of the capital charges on working capital and total start-up expenses loan, taken here as 0.05. As in the case of the cost items of C_{CAPEX}, the remaining items of C_{FCP} are estimated based on the superordinate OPEX cost items $C_{OPEX,i}$ and their respective Lang factors $f_{OPEX,i}$, as indicated in Table 5.

By-product revenues (R_{H_2}) considered in this study correspond to the income generated by the sale of the produced H_2 during the PEME plant lifetime. In the same way as with the costs for deionized water, liquid O_2, and electricity, R_{H_2} is calculated based on the simulation results for yearly H_2 production ($\sum \dot{m}^{EZ}_{H_2,eff}$) and the specific selling or market price c_{H_2} (also see Section 2.4.2). The yearly amount of produced H_2 is also assumed to remain constant until the plants reach EOL.

In order to calculate the C_{NCP} of electrolysis O_2, the annuity method based on the total spent fixed capital investment costs C_{FCI} is applied. The total C_{FCI} is annualized by determining the annual capital charge (C_{ACC}) required to fully reimburse the initial capital investment until the plants reach EOL. As a result, the fixed capital investments after interest ($C_{FCI,ai}$), also known as depreciation costs, are determined:

$$C_{FCI,ai} = y_{PL} \cdot \underbrace{C_{FCI} \cdot \frac{i_c (i_c + 1)^{y_{PL}}}{(i_c + 1)^{y_{PL}} - 1}}_{\substack{Annual\ capital \\ charge\ (C_{ACC})}} \quad (21)$$

The FCI are financed by debt and equity represented by a compound interest rate i_c (also weighted average cost of capital; see Equation (22)) with respective interest rates

for debt i_d and equity i_e, as well as a specific debt ratio r_d for both capital sources. In the present studies, i_e is taken as 0.1 and r_d as 0.5, resulting in an i_c value of 0.075.

$$i_c = r_d \cdot i_d + (1 - r_d) \cdot i_e \tag{22}$$

Based on the retrieved values of $C_{FCI,ai}$ and C_{OPEX}, as well as potential revenues (R_S) from plant salvage (PEME stacks) at plant EOL and the cumulative annual O_2 production ($\sum \dot{m}_{O_2,eff}^{EZ}$), the net costs of O_2 production (C_{NCP}) are determined (Equation (23)).

$$C_{NCP} = \frac{C_{FCI,ai} + C_{OPEX} - R_S}{y_{PL} \cdot \sum \dot{m}_{O_2,eff}^{EZ}} \tag{23}$$

The chosen annuity approach assumes that investments and cash flows start immediately and, due to the integral nature of this approach, no specific timing of investments and revenues has been considered. Moreover, taxes and depreciation charges have been neglected in the annuity approach and hence the determination of C_{NCP}. Revenues from PEME stack salvage are only considered if the remaining lifetime of the installed PEME stack at EOL is larger than 8000 h. The salvage value is derived from the initial stack investment costs, the ratio of the remaining and initial stack lifetime (y_{PEME}), as well as an additional salvage factor of 0.5.

In addition to the annuity method, the potential specific minimum selling price of O_2 through the PEME plant (c_{MSP,O_2}) is calculated via a cash flow analysis, i.e., determination of the net present value (NPV) at the plant EOL. With the annual gross profit (P_n), the depreciation tax allowances (D_n), and the corporate tax rate (t_{cp}), the annual cash flow (CF_n) in each year n can be assessed (Equations (24) and (25)). Subsequently, the NPV is calculated based on Equation (26). To comply with the initial assumption of an NPV of zero at the plant's EOL, c_{MSP,O_2} is varied via a simple search algorithm until the condition formulated in Equation (26) is reached.

$$P_n = c_{MSP,O_2} \cdot \sum \dot{m}_{O_2,eff}^{EZ} + c_{H_2} \cdot \sum \dot{m}_{H_2,eff}^{EZ} + \frac{R_S - C_{VCP} - C_{FCP}}{y_{PL}} \tag{24}$$

$$CF_n = P_n \cdot (1 - t_{cp}) + D_n \cdot t_{cp} \tag{25}$$

$$NPV = \sum_{n=1}^{y_{PL}} \frac{CF_n}{(1 + i_c)^n} = 0 \tag{26}$$

A straight-line depreciation over 10 years and a corporate tax rate (t_{cp}) of 0.3 are assumed. All capital expenses are spent in year zero. The TEA studies are carried out within the software framework of MATLAB R2017b.

2.4.2. Cost Inventory and Market Analysis

To provide economic data for the calculations described in Section 2.4.1 and allow for the realization of the TEA under various conditions, a cost inventory for the items with significant impact on the economic performance of the PEME plant has been defined. The items selected for the cost inventory include the following:

- Electricity price (LCOE) depending on the source of origin.
- Selling price of produced H_2 depending on market conditions.
- Price of O_2 from conventional sources.
- The investment and replacement costs attributed to the PEME.

The presented TEA is performed for the reference year 2020 based on current data and also for 2030 based on forecasts presented in literature to reflect the development of the process's economics. Three different sets of economic parameters have been defined for each of the selected years in order to represent optimistic, neutral, and pessimistic

economic conditions for the project's implementation. Four different electricity sources have been considered in the present study, namely conventional, PV, and wind (off-shore and on-shore) energy plants. The costs defined for the different items in the cost inventory, as well as the PEME stack lifetime y_{PEME}, are presented in Table 6. For 2020, the plant's lifetime y_{PL} is assumed to be 20 years, while for 2030, it is assumed to be 30 years.

Table 6. Cost inventory for the estimation of net costs of production (NCP) for electrolysis O_2 based on reference values taken from literature [36–42].

		2020			2030		
		Optimistic	**Neutral**	**Pessimistic**	**Optimistic**	**Neutral**	**Pessimistic**
LCOE c_E ($€\cdot MWh^{-1}$)	Conventional	31	43	55	47	71	94
	PV	31	57	140	21	51	81
	Wind on shore	39	61	83	25	53	81
	Wind off shore	72	105	138	56	78	101
H_2 price c_{H_2} ($€\cdot kg^{-1}$)		6	5	4	4	3	2
PEME stack lifetime y_{PEME} (h)		67,500	59,000	50,500	85,000	75,500	66,125
PEME stack cost c_{PEME} ($€\cdot kW^{-1}$)		867	1000	1225	453	600	780
O_2 price $c_{O_2,ext}$ ($€\cdot t^{-1}$)		100	100	100	134 [a]	122 [b]	110 [c]

[a] annual price increase of 3%, [b] annual price increase of 2%, [c] annual price increase of 1%.

The projections of the cost inventory reflect the trends reported in the literature [36–42]. While electricity prices for all renewable sources are expected to decrease, the price for conventional sources is expected to increase due to higher costs for CO_2 emission certificates. Improvements in electrolyser performance and the corresponding decrease in investments are expected to result in decreasing H_2 selling prices in 2030. It is important to point out that, although a stronger reduction in H_2 production costs would be a positive trend regarding the transition to a sustainable energy system, this would increase the calculated NCP for O_2, and therefore the pessimistic scenario considers lower H_2 selling prices. Conventional O_2 prices are assumed to increase at a different rate for each economic condition. The cost of deionized water c_{H_2O} is also assumed to increase with time, taking a value of 2 $€\cdot m^{-3}$ and 3 $€\cdot m^{-3}$ in 2020 and 2030, respectively.

3. Results and Discussion

3.1. O_2 Demand of the BSM2 WWTP

The behaviour of the O_2 demand of the AS system in the BSM2 can be seen in Figure 2 after converting $\dot{n}^{AS}_{O_2,eff}$ to $kg\cdot d^{-1}$ ($\dot{m}^{AS}_{O_2,eff}$). The average daily O_2 demand for the BSM2 was calculated at 10,388 $kg\cdot d^{-1}$. The use of larger DO_{sat} values to account for the use of pure O_2 (see Section 2.2.) results in higher transfer rates OTR for a given k_La and measured DO concentration when compared with air (see Equation (1)). The k_La values calculated by the PI controller are therefore lower in this study than in the original BSM2, i.e., less gas volume and therefore less energy for gas injection is required when using pure O_2. When k_La values are too low, the additional mixing energy for maintaining the sludge in suspension in the nitrification tanks is to be calculated as part of the operational costs in the BSM2 [18]. However, since the TEA scope includes only the PEME plant, these effects of pure O_2 use on the operational costs of WWTP are not further assessed.

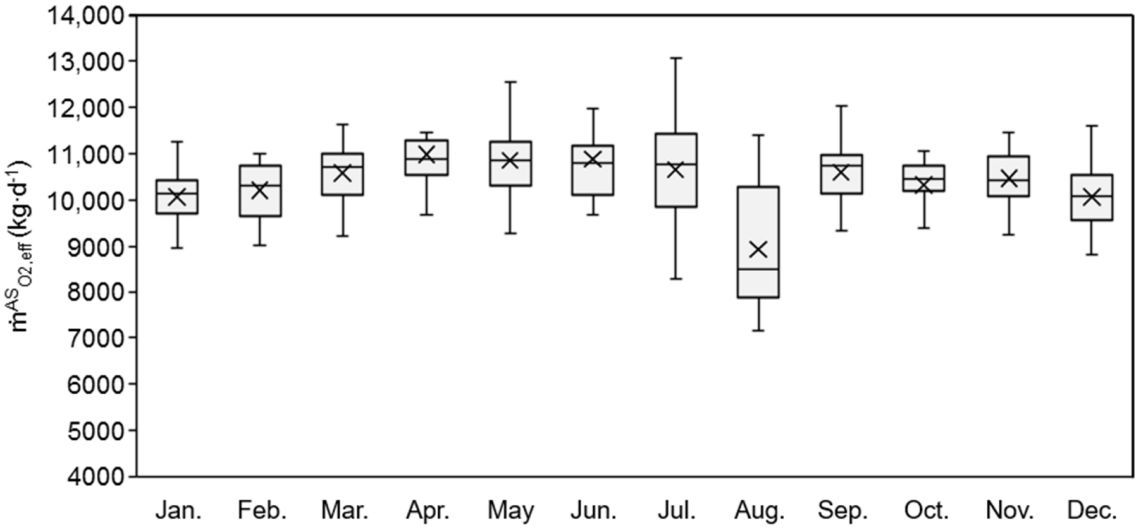

Figure 2. Daily O_2 demand from the AS system of the BSM2 plant. Average values are represented by an ×, median values by a line, the limits of the boxes are the first and third quartile, and outliers are excluded.

The effect of seasonal changes can be seen in higher O_2 demand during warmer months, which can be explained by the decrease in DO_{sat} at higher temperatures and the corresponding decrease in the amount of O_2 that can be maintained in the water phase. A further seasonal effect that can be seen in Figure 2 is the decrease in O_2 demand caused by less household wastewater production during the summer holiday season [19]. Intraday variations in O_2 demand follow the profile of wastewater inflow into the WWTP, i.e., are higher during daytime with peaks around midday and in the evening (see Figure 3).

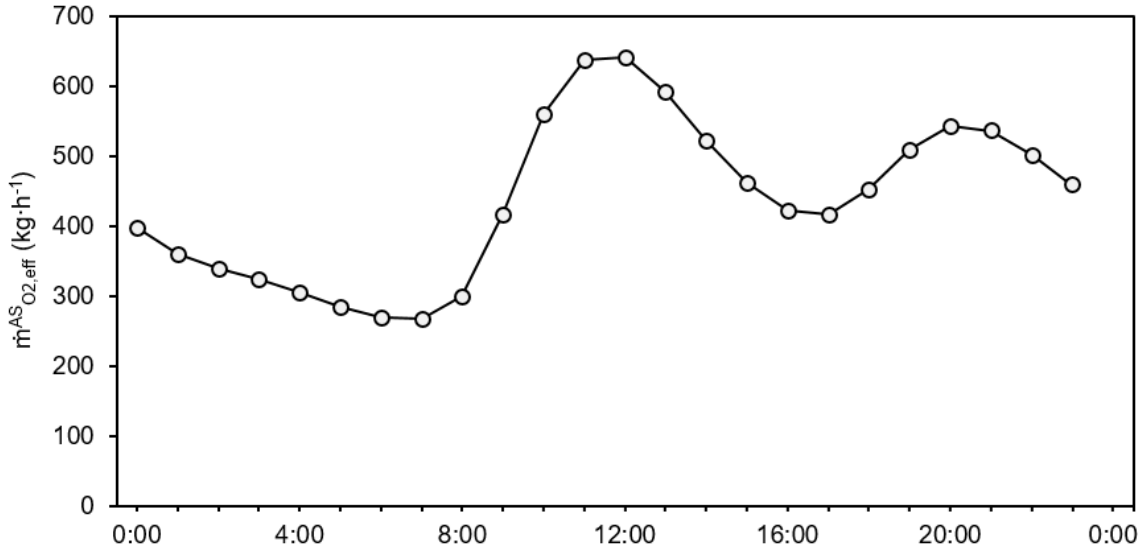

Figure 3. Intraday O_2 demand from the AS system of the BSM2 plant.

The cumulative histogram for $\dot{m}^{AS}_{O_2,eff}$ can be seen in Figure 4, showing that during 80% of the simulation time, the O_2 demand is between approx. 9200 and 11,300 kg·d^{-1}.

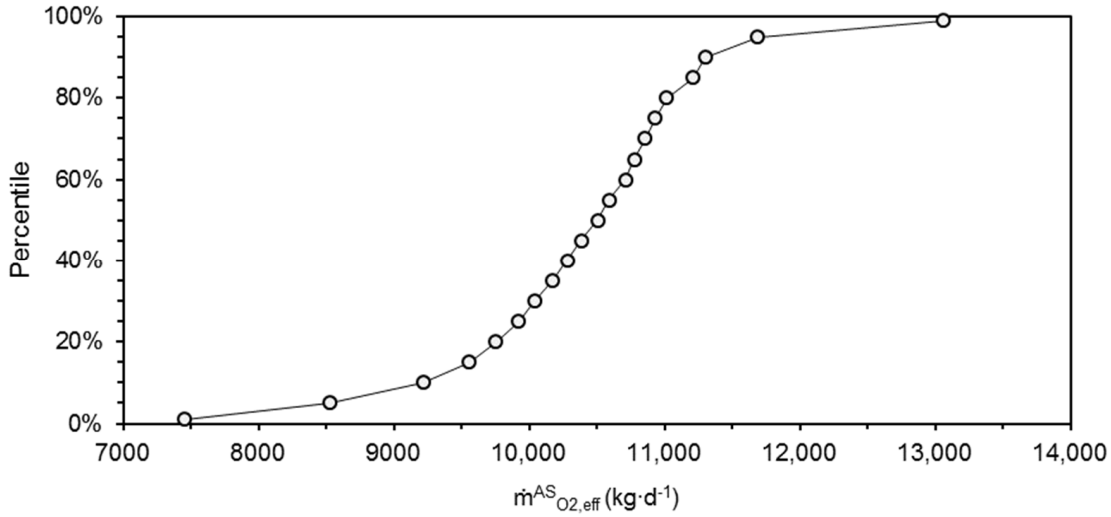

Figure 4. Histogram of daily O_2 demand from the AS system of the BSM2 plant.

3.2. Dimensioning of PEME Plant

The selected capacities of the PEME plant components for each scenario and the corresponding simulation results are shown in Table 7. The operation cycles defined in Section 2.3 are subject to changes due to the activation of the interlock, resulting in an effective amount of hours at full load $t_{FLH,eff}$ that differs from the $t_{FLH,nom}$ presented in Table 1. When analysing gas production, it can be seen that the difference in PEME capacity between both scenarios is compensated by the difference in $t_{FLH,real}$, resulting in a very similar production of H_2 and O_2. In both scenarios, there are periods where, despite the activation of the interlock, the O_2 flowrate produced by the PEME at full load capacity is under the O_2 demand, resulting in p_{sto} values below p_{min} and the need to supply O_2 from the contingency tank. The higher PEME capacity and storage tank volume in scenario 1 results in a significantly shorter period with p_{sto} below p_{min} when compared with scenario 2, leading to a larger volume of the contingency tank in scenario 2. These critical periods are, however, relatively short; in both scenarios, the PEME plant is capable of supplying enough O_2 to the BSM2 WWTP during more than 99% of the simulated time without recurring to the contingency tank. For neither of the scenarios is there a period where p_{sto} is above p_{max}.

Table 7. Result of the dimensioning of the PEME plant for both scenarios.

Parameter	Scenario 1	Scenario 2
n_c (-)	1350	1000
P_{PEME} (kW)	6400	4750
P_{comp} (kW)	37	27
V_{sto} (m^3)	250	200
V_{cont} (m^3)	5	28
Effective % of time at full load	47	72
$t_{FLH,eff}$ ($h \cdot a^{-1}$)	4073	6259
$\sum \dot{m}_{O_2,eff}$ ($t \cdot a^{-1}$)	3782	3780
$\sum \dot{m}_{H_2,eff}$ ($t \cdot a^{-1}$)	476	476
Time with $p_{sto} < p_{min}$ ($d \cdot a^{-1}$)	0.4	2.5
Time with $p_{sto} > p_{max}$ ($d \cdot a^{-1}$)	0	0

3.3. Economic Assessment

The cost breakdown of all relevant cost categories of purchased equipment costs C_{PEC}, total capital expenses C_{CAPEX}, operational costs C_{OPEX}, as well as the net O_2 production costs C_{NCP} are presented in Figure 5 for an exemplary case (scenario 1 in 2020, under neutral

economic conditions and supplied with PV electricity). The breakdowns shown in Figure 5a to 5e are representative for all other assessed cases, i.e., the proportion of cost items is similar. In all cases, C_{PEC} is dominated by the initial PEME investment cost (between 53.2% and 73.4% of C_{PEC} for scenario 1 and between 50.7% and 71.5% for scenario 2), followed by the investments for O_2 tanks, the converter, and the compressor. The share of C_{PEC} made up by PEME investment costs is between 13.2% and 7.5% lower in 2030 than in 2020 due to the assumed decrease in the PEME stack price. C_{FCI}, which make up 92.7% of C_{CAPEX}, are dominated by investments inside battery limits C_{ISBL} (47.8%) and the costs of design and engineering C_{DE} (36.8%).

Figure 5. Breakdown of (**a**) purchased equipment costs C_{PEC}; (**b**) fixed costs of investment C_{FCI}; (**c**) capital expenditures C_{CAPEX}; (**d**) variable costs of production C_{VCP}; (**e**) fixed costs of production C_{FCP} and; (**f**) net costs of production C_{NCP} for scenario 1 in 2020, neutral economic conditions, and PV electricity supply.

The costs of electricity consistently make up more than 85% of C_{VCP}. The cost share of PEME stack replacement in C_{VCP} is always below 10%, while the sum of the shares of deionized water and external O_2 for the contingency tank is always below 3%. Capital charges on working capital and total start-up expenses make up the majority of the fixed costs of production C_{FCP} (between 50 and 59.8%).

An overview of all calculated C_{NCP} after revenues are presented in Table 8. Lower investment costs for the PEME stacks result in overall lower C_{NCP} for scenario 2. In 2020, all calculated C_{NCP} are higher than the price of O_2 from conventional sources (100 €·t^{-1}).

In 2030 and under positive economic conditions, competitive production costs below or near the conventional O_2 price (134 €·t^{-1}) are achieved for the PEME plant designed according to scenario 2 and supplied by PV (128 €·t^{-1}) and wind on-shore electricity (161 €·t^{-1}). Such relatively low C_{NCP} are the result of optimistic trends regarding costs of PEME stacks and renewable electricity supply.

Table 8. Calculated net costs of production C_{NCP} in €·t^{-1}.

Year	Scenario	Electricity Source	Optimistic	Neutral	Pessimistic
2020	Scenario 1	Conventional	500	830	1232
		PV	500	945	1935
		Wind on shore	566	978	1464
		Wind off shore	839	1342	1919
	Scenario 2	Conventional	286	609	977
		PV	286	727	1693
		Wind on shore	353	761	1212
		Wind off shore	631	1131	1676
2030	Scenario 1	Conventional	452	874	1311
		PV	237	709	1203
		Wind on shore	270	725	1203
		Wind off shore	526	932	1369
	Scenario 2	Conventional	347	751	1165
		PV	128	582	1055
		Wind on shore	161	599	1055
		Wind off shore	423	810	1224

As can be seen in Figure 5f, C_{NCP} are dominated by fixed costs of investments, the interest on these investments, and electricity costs. However, the share of electricity costs in C_{NCP} varies greatly among the analysed cases (between 20.2 and 51.5% in scenario 1 and between 25 and 57.6% in scenario 2). In 2020, the difference between optimistic and pessimistic PV electricity costs is largest among all energy sources considered (see Table 6). For this reason, both the highest and lowest C_{NCP} values in 2020 correspond to the PV electricity supply. In 2030, the costs of PV and wind on-shore electricity are very similar, with PV resulting in slightly lower C_{NCP}, while more expensive conventional and wind off-shore electricity supply results in higher production costs. The sum of all cost items aside from electricity, C_{FCI}, and interests on C_{FCI} consistently make up less than 10% of C_{NCP}.

It is important to consider that items in the cost inventory were all assigned either optimistic, neutral, or pessimistic values in each case (see Table 6); thus, the results presented in Table 8 do not include combinations of economic conditions. For example, if optimistic values are selected for the cost of PV electricity and the selling price of H_2 in 2030 while pessimistic values are kept for all other items in the cost inventory, the resulting C_{NCP} for scenario 2 would be 296 €·t^{-1} rather than 1055 €·t^{-1}.

The maximum and minimum calculated potential O_2 selling prices c_{MSP,O_2} are shown in Table 9. Values for c_{MSP,O_2} are always higher than C_{NCP} since plant depreciation and tax on income are included in their calculation (see Equation (24)). The obtained selling prices are therefore not competitive with conventional O_2 sources with prices of 100 €·t^{-1} (2020) and 134 €·t^{-1} (2030) in any of the studied cases.

Table 9. Range of calculated minimum selling prices c_{MSP,O_2} in €·t^{-1}.

	Scenario 1		Scenario 2	
	2020	2030	2020	2030
c_{MSP,O_2} max.	2184	1525	1882	1343
c_{MSP,O_2} min.	695	350	436	215

3.4. Further Research

The present study offers a methodology for the analysis of the economics of O_2 valorisation in biological treatment steps of WWTPs based on a recognized benchmark such as the BSM2 and simple models for the components of a PEME plant. Regarding

possible subjects for further investigations, in this study both the efficiency factor used to represent O_2 losses in gas separation steps η_p and the OTE of the oxygenation system installed at the WWTP are taken as constant. New developments in gas separation units and oxygenation systems are expected to lead to higher efficiencies [43,44], which in turn would help to reduce C_{NCP}. Furthermore, many of the AS systems using pure O_2 are designed with a closed headspace to enable the collection and reuse of injected O_2 [12], which would result in lower electrolyser capacities being required. Future TEAs could address a closed AS system, however additional effects of closed headspace design such as the inhibition of nitrification processes due to CO_2 accumulation and pH decrease should also be considered [12,45,46]. The costs for the adaption of the WWTP infrastructure to the use of pure O_2 should also be analysed.

Further effects of pure O_2 in biological and chemical processes in AS systems are outside the scope of this study. These include benefits such as reduction in sludge production, reduction in fouling foaming and improvements in treatment efficiency [12,13]. Such effects of the use of pure O_2 from electrolysers in AS systems should therefore also be investigated experimentally. Possible synergies between electrolyser plants and other processes in WWTPs can be considered in future simulation studies. These may include the use of heat recovered from the electrolysers cells or the methanation of biogas produced in sludge treatment with the H_2 from the electrolyser [10].

The dimensioning of the PEME plant was done to cover the whole O_2 demand from the BSM2 WWTP with a capacity of 80,000 PE. In Germany this correspond to the second largest category for WWTP capacity defined by the national environment agency. More than 60% of wastewater in Germany is treated at WWTPs with installed capacities above 10,000 PE, although these larger plants make less than 10% of the total number of WWTPs [47]. The proposed methodology can be applied to analyse the economics of similar projects to fully supply smaller WWTPs or partially cover the O_2 demand in larger ones (e.g., pre-treatment step with pure O_2 before conventional AS system supplied with air). A rough estimation of the required PEME capacity for a smaller WWTP of 10,000 PE treating wastewater with a typical O_2 demand of 1200 kg $O_2 \cdot d^{-1}$ [48] can be done by a lineal extrapolation of the PEME capacities presented in Section 3.2. This results in a required capacity of around 740 kW for scenario 1 and 550 kW for scenario 2. The use of pure O_2 is recommended for the treatment of highly-strength wastewater [12], thus future analyses should be done by using models of industrial WWTPs. The same is true for membrane bioreactors (MBR), for which the use of pure O_2 has been shown to increase treatment efficiency and reduce membrane fouling [49].

Regarding the analysed economic conditions, further investigations could integrate changes in electricity prices during the simulated period. In future renewable-based electricity networks, the operation of electrolysers can be adjusted through demand side management according to prices and availability of energy [16]. Within a flexible electricity pricing scheme, plants operators could benefit from reduced electricity costs by adjusting the operation scheme of the PEME accordingly while at the same time providing network regulation services. Moreover, analyses in this study do not consider variations in the cost inventory during the plants lifetime; the prices and performance of the PEME plant are assumed constant until EOL for simplification. More detailed consideration of the H_2 valorisation processes should also be included in future studies (e.g., variations in sold amount and price or the implementation of internal valorisation measures).

4. Conclusions

Power-to-gas technologies based on water electrolysis are expected to play a central role in future renewable energy networks, where green H_2 and derived synthetic fuels are used as alternatives to fossil fuels. In the electrolysis process, large amounts of O_2 are produced alongside H_2, however O_2 is usually seen as a by-product and discarded into the atmosphere. In the present study the economics of the valorisation of electrolysis O_2 in

biological treatment steps of municipal WWTPs has been analysed based on the results of mathematical simulation models.

The operation WWTP of the BSM2 has been modelled alongside a PEME system and used to simulate O_2 supply for an operation period of one year. Two scenarios regarding full load hours per year and corresponding PEME plant dimensions have been considered. Simulation data on the amount of consumables required and the produced gas flowrates was used as an input for a TEA on the net costs of O_2 production NCP, assuming that the produced H_2 is sold to a nearby industry. The TEA was performed for the years 2020 and 2030 under sets of optimistic, neutral and pessimistic conditions regarding costs and revenue streams.

Simulation results show that for 80% of the simulation period the O_2 demand of the AS of the BSM2 plant is between approx. 9200 and 11,300 $kg \cdot d^{-1}$. The dimensions of the PEME stack and amount of full load hours were 6.4 MW and 4073 $h \cdot a^{-1}$ for scenario 1, whereas 4.8 MW and 6259 $h \cdot a^{-1}$ for scenario 2. The PEME plants in both scenarios were able to cover the O_2 demand for more than 99% of the simulated time without having to rely on contingency O_2 storage. The results of the TEA show that NCP are dominated by the investment and respective interests on the PEME stacks, as well as the electricity costs. The sum of other cost components makes less than 10% of the NCP. Although for the year 2020 NCP for O_2 produced by the PEME plant are higher than references for the costs of industrial O_2, in 2030 the combination of lower investment costs for PEME stacks and lower renewable electricity prices (PV and wind on shore) resulted in competitive electrolysis O_2 costs when assuming optimistic economic conditions.

Further studies can follow the approach described here to analyse the economics of electrolysis O_2 supply to conventional WWTPs of different size or different systems such as MBRs. The simple models for the PEME plant and the O_2 supply process described here should also be expanded to include the effects of using pure O_2 in AS system, more detailed considerations regarding H_2 valorisation, as well as changes in electricity prices and system performance during the plants lifetime. The use of electrolysers at WWTPs for demand side management by adjusting the operation according to the energy networks behaviour should also complement the presented results.

Author Contributions: Conceptualization, M.A.P.R., S.F.R., S.F. and U.H.; methodology, M.A.P.R. and S.F.; software, M.A.P.R. and S.F.; formal analysis, M.A.P.R. and S.F.; investigation, M.A.P.R. and S.F.; writing—original draft preparation, M.A.P.R. and S.F.; writing—review and editing, S.F.R. and U.H.; visualization, M.A.P.R. and S.F.; supervision, S.F.R. and U.H.; project administration, S.F.R. and U.H.; funding acquisition, S.F.R. and U.H. All authors have read and agreed to the published version of the manuscript.

Funding: This work is partly funded by the Initiative and Networking Fund of the Helmholtz Association in the frame of the Clean Water Technology Lab CLEWATEC—a Helmholtz Innovation Lab under the reference number HIL-A02. The authors are responsible for the content of this publication.

Data Availability Statement: The data presented in this study are openly available in RODARE–Rossendorf Data Repository at http://doi.org/10.14278/rodare.2274.

Acknowledgments: The authors would like to thank Michael Ogurek and Gloria Robleto for the support in the implementation of the models into the SIMBA software. Additionally, the authors would like to thank Anjan Goswami for the contributions made to the implementation of the models as part of his internship at HZDR.

Conflicts of Interest: The authors declare no conflict of interest. In addition, the funders had no role in the design of the study; in the collection, analyses, or interpretation of data; in the writing of the manuscript, or in the decision to publish the results.

Abbreviations and Acronyms

AC/DC	Alternating Current/Direct Current
ACC	Annual Capital Charge
AS	Activated Sludge
ASM1	Activated Sludge Model No. 1
BSM2	Benchmark Simulation Model No. 2
CC	Contingency Charges
CAPEX	Capital Expenditures
CEPCI	Chemical Engineering Plant Cost Index
DE	Design and Engineering
DSO	Direct Salary Overhead
EOL	End of Lifetime
EV	Environmental Charges
FCI	Fixed Capital Investment
FCP	Fixed Costs of Production
HZDR	Helmholtz-Zentrum Dresden-Rossendorf
ISBL	Inside Battery Limits
IWA	International Water Association
LCOE	Levelized Cost of Energy
MBR	Membrane Bioreactor
MT	Maintenance
NCP	Net Costs of Production
NPV	Net Present Value
OL	Operating Labour
OPEX	Operational Expenditures
OSBL	Outside Battery Limits
OTE	Oxygen Transfer Efficiency
OTR	Oxygen Transfer Rate
PE	Population Equivalent
PEC	Purchased Equipment Costs
PEM	Proton Exchange Membrane
PEME	Proton Exchange Membrane Electrolyser
PI	Proportional Integer Controller
PTI	Property Taxes and Insurance
PV	Photovoltaic
ROL	Rent of Land
SE	Start-Up Expenses
SV	Supervision
TEA	Techno-Economic Assessment
VCP	Variable Costs of Production
WC	Working Capital
WWTP	Wastewater Resource Recovery Facility

Symbols

a_c	Active cell area of the electrolyser
$a_{T,i}$	Scaling parameter of storage tank i
$b_{T,i}$	Scaling parameter of storage tank i
c_E	Specific electricity costs
c_{H_2}	Specific hydrogen selling price
c_{H_2O}	Specific feed water costs electrolyser
c_{MSP,O_2}	Minimum selling price of oxygen
$c_{O_2,ext}$	Specific costs of oxygen from external sourcing
c_{PEME}	Specific electrolyser cost
C_E	Total electricity costs

$C_{FCI,ai}$	Fixed capital investments after interest payments
C_{H_2O}	Total feed water costs electrolyser
C_i	Total costs of component i
$C_{i,base}$	Total costs (base year) of component i
$C_{O_2,ext}$	Total costs of oxygen from external sourcing
$C_{R,PEME}$	Total replacement costs electrolyser stacks
$C_{T,i}$	Total costs of storage tank i
$CEPCI$	CEPCI of the estimation year
$CEPCI_{base}$	CEPCI of the base year
CF_n	Annual cash flow
D_n	Annual depreciation tax allowances
DO	Dissolved oxygen
DO_{sat}	Saturation oxygen concentrations
$f_{CAPEX,i}$	Lang factor of CAPEX cost item i
$f_{OPEX,i}$	Lang factor of OPEX cost item i
F	Faraday constant
i_c	Compound interest rate
i_d	Interest rate debt
i_e	Interest rate equity
J	Average current density
k_La	Volumetric oxygen transfer coefficient
M_{O_2}	Molar mass oxygen
$\dot{m}^{AS}_{O_2,eff}$	Effective mass flow into the liquid phase (activated sludge)
$\dot{m}^{EZ}_{H_2,eff}$	Effective mass production rate hydrogen (electrolyser)
n	Year (for NPV analysis)
n_c	Number of electrolyser cells
$n_{T,i}$	Number of subordinate single tanks of storage tank i
$\dot{n}_{O_2,ext}$	Required external molar oxygen intake (contingency tank)
$\dot{n}^{AS}_{O_2,nom}$	Nominal molar flow into the liquid phase (activated sludge)
$\dot{n}^{AS}_{O_2,eff}$	Effective molar flow into the liquid phase (activated sludge)
$\dot{n}^{EZ}_{H_2,nom}$	Nominal molar production rate hydrogen (electrolyser)
$\dot{n}^{EZ}_{H_2,eff}$	Effective molar production rate hydrogen (electrolyser)
$\dot{n}^{EZ}_{H_2O}$	Molar consumption of deionized water (electrolyser)
$\dot{n}^{EZ}_{O_2,nom}$	Nominal molar production rate oxygen (electrolyser)
$\dot{n}^{EZ}_{O_2,eff}$	Actual molar production rate oxygen (electrolyser)
OTE	Oxygen transfer efficiency
OTR	Oxygen transfer rate
p_{PEME}	Electrolyser pressure
p_{max}	Maximum pressure intermediate oxygen tank
p_{min}	Minimum pressure intermediate oxygen tank
p_{sto}	Pressure intermediate oxygen storage tank
P_{comp}	Compressor power
P_n	Annual gross profit
P_{PEME}	Electrolyser power
r_d	Debt ratio
R	Universal gas constant
R_{H_2}	By-product revenue H_2
R_S	Revenue of plant salvage
S_i	Actual scale of component i
$S_{i,base}$	Reference scale of component i in the base year
$S_{T,i}$	Scale of storage tank i
t_{cp}	Corporate tax rate
$t_{FLH,nom}$	Nominal full load hours
$t_{FLH,eff}$	Effective full load hours
T_{PEME}	Electrolyser temperature
T_{sto}	Temperature intermediate oxygen storage tank

$V_{AS,i}$	Volume of nitrification tank i
V_{cont}	Volume contingency oxygen storage tank
V_{sto}	Volume intermediate oxygen storage tank
y_{PEME}	PEM electrolyser stack lifetime
y_{PL}	Plant lifetime
α	Alpha factor
δ_i	Scaling exponent of component i
$\delta_{T,i}$	Scaling exponent of tank i
η_f	Faradaic efficiency
η_{comp}	Compressor efficiency
η_p	Efficiency factor electrolysis
κ	Polytropic exponent
φ_{EZ}	Cell voltage
$\sum \dot{m}^{EZ}_{H_2,eff}$	Cumulative annual H_2 production
$\sum \dot{m}^{EZ}_{O_2,eff}$	Cumulative annual O_2 production

References

1. Staffell, I.; Pfenninger, S. The increasing impact of weather on electricity supply and demand. *Energy* **2018**, *145*, 65–78. [CrossRef]
2. Kanellopoulos, K.; Blanco, H. The potential role of H2 production in a sustainable future power system—An analysis with METIS of a decarbonised system powered by renewables in 2050. *Eur. Comm. JRC Tech. Rep.* **2019**, *10*, 540707. [CrossRef]
3. Glenk, G.; Reichelstein, S. Economics of converting renewable power to hydrogen. *Nat. Energy* **2019**, *4*, 216–222. [CrossRef]
4. BMU Nationale Wasserstrategie—Entwurf des Bundesumweltministeriums. Bonn, 2021. Available online: www.bmu.de (accessed on 28 October 2021).
5. IRENA. Green Hydrogen Cost Reduction—Scaling Up Electrolysers to Meet the 1.5 °C Climate Goal. Abu Dhabi, 2020. Available online: https://www.irena.org/-/media/Files/IRENA/Agency/Publication/2020/Dec/IRENA_Green_hydrogen_cost_2020.pdf (accessed on 25 February 2022).
6. Holst, M.; Aschbrenner, S.; Smolinka, T.; Voglstätter, C.; Grimm, G. Cost forecast for low temperature electrolysis—Technology driven bottom-up prognosis for PEM and alkaline water electrolysis systems. Freiburg, 2021. Available online: https://www.ise.fraunhofer.de/content/dam/ise/de/documents/publications/studies/cost-forecast-for-low-temperature-electrolysis.pdf (accessed on 17 October 2022).
7. Schäfer, M.; Gretzschel, O.; Steinmetz, H. The possible roles of wastewater treatment plants in sector coupling. *Energies* **2020**, *13*, 2088. [CrossRef]
8. DWA. DWA Wasserstoff trifft Abwasser—Arbeitsbericht der DWA-Arbeitsgruppe KEK-7.1 "Wasserstoffbasierte Energiekonzepte". *KA Korrespondenz Abwasser* **2022**, *7*, 597–605.
9. Calbry-Muzyka, A.S.; Schildhauer, T.J. Direct Methanation of Biogas—Technical Challenges and Recent Progress. *Front. Energy Res.* **2020**, *8*, 570887. [CrossRef]
10. Michailos, S.; Walker, M.; Moody, A.; Poggio, D.; Pourkashanian, M. A techno-economic assessment of implementing power-to-gas systems based on biomethanation in an operating waste water treatment plant. *J. Environ. Chem. Eng.* **2021**, *9*, 104735. [CrossRef]
11. Gretzschel, O.; Schfer, M.; Steinmetz, H.; Pick, E.; Kanitz, K.; Krieger, S. Advanced wastewater treatment to eliminate organic micropollutants in wastewater treatment plants in combination with energy-efficient electrolysis at WWTP Mainz. *Energies* **2020**, *13*, 3599. [CrossRef]
12. Skouteris, G.; Rodriguez-Garcia, G.; Reinecke, S.F.; Hampel, U. The use of pure oxygen for aeration in aerobic wastewater treatment: A review of its potential and limitations. *Bioresour. Technol.* **2020**, *312*, 123595. [CrossRef]
13. Mohammadpour, H.; Cord-Ruwisch, R.; Pivrikas, A.; Ho, G. Utilisation of oxygen from water electrolysis—Assessment for wastewater treatment and aquaculture. *Chem. Eng. Sci.* **2021**, *246*, 117008. [CrossRef]
14. Hu, Y.-Q.; Wei, W.; Gao, M.; Zhou, Y.; Wang, G.-X.; Zhang, Y. Effect of pure oxygen aeration on extracellular polymeric substances (EPS) of activated sludge treating saline wastewater. *Process Saf. Environ. Prot.* **2019**, *123*, 344–350. [CrossRef]
15. García-Valverde, R.; Espinosa, N.; Urbina, A. Simple PEM water electrolyser model and experimental validation. *Energy* **2012**, *37*, 1927–1938. [CrossRef]
16. Allidières, L.; Brisse, A.; Millet, P.; Valentin, S.; Zeller, M. On the ability of PEM water electrolysers to provide power grid services. *Int. J. Hydrogen Energy* **2019**, *44*, 9690–9700. [CrossRef]
17. SIMBA# | ifak Magdeburg. Available online: https://www.ifak.eu/de/produkte/simba (accessed on 18 October 2022).
18. Gernaey, K.V.; Jeppsson, U.; Vanrolleghem, P.A.; Copp, J.B. *Benchmarking of Control Strategies for Wastewater Treatment Plants*; IWA Publishing: London, UK, 2015.
19. Gernaey, K.; Flores-Alsina, X.; Rosen, C.; Benedetti, L.; Jeppsson, U. Dynamic influent pollutant disturbance scenario generation using a phenomenological modelling approach. *Environ. Model. Softw.* **2011**, *26*, 1255–1267. [CrossRef]

20. Stenstrom, M.K.; Kido, W.; Shanks, R.F.; Mulkerin, M. Estimating oxygen transfer capacity of a full-scale pure oxygen activated sludge plant. *J. Water Pollut. Control Fed.* **1989**, *61*, 208–220.
21. Lide, D. *CRC Handbook of Chemistry and Physics*, 84th ed.; CRC Press: Boca Raton, FL, USA, 2004.
22. Wang, L.K.; Shammas, N.K.; Hung, Y.-T. *Advanced Biological Treatment Processes*; Springer Science & Business Media: Totowa, NJ, USA, 2010; Volume 9.
23. Lehner, F.; Hart, D. Chapter 1—The importance of water electrolysis for our future energy system. In *Electrochemical Power Sources: Fundamentals, Systems, and Applications*; Smolinka, T., Garche, J., Eds.; Elsevier: Amsterdam, The Netherlands, 2022; pp. 1–36.
24. Carmo, M.; Fritz, D.L.; Mergel, J.; Stolten, D. A comprehensive review on PEM water electrolysis. *Int. J. Hydrogen Energy* **2013**, *38*, 4901–4934. [CrossRef]
25. Bertuccioli, L.; Chan, A.; Hart, D.; Lehner, F.; Madden, B.; Standen, E. Development of Water Electrolysis in the European Union. Lausanne, 2014. Available online: https://refman.energytransitionmodel.com/publications/2020 (accessed on 9 February 2023).
26. Rizwan, M.; Alstad, V.; Jäschke, J. Design considerations for industrial water electrolyzer plants. *Int. J. Hydrogen Energy* **2021**, *46*, 37120–37136. [CrossRef]
27. Towler, G.; Sinnott, R. *Chemical Engineering Design—Principles, Practice and Economics of Plant and Process Design*, 2nd ed.; Elsevier: Oxford, UK, 2013.
28. The Chemical Engineering Plant Cost Index—Chemical Engineering. Available online: https://www.chemengonline.com/pci-home (accessed on 19 October 2022).
29. Plant Cost Index Archives—Chemical Engineering. Available online: https://www.chemengonline.com/site/plant-cost-index/ (accessed on 19 October 2022).
30. Schmidt, O.; Gambhir, A.; Staffell, I.; Hawkes, A.; Nelson, J.; Few, S. Future cost and performance of water electrolysis: An expert elicitation study. *Int. J. Hydrogen Energy* **2017**, *42*, 30470–30492. [CrossRef]
31. Fu, Q.; Mabilat, C.; Zahid, M.; Brisse, A.; Gautier, L. Syngas production via high-temperature steam/CO_2 co-electrolysis: An economic assessment. *Energy Environ. Sci.* **2010**, *3*, 1382–1397. [CrossRef]
32. De Saint Jean, M.; Baurens, P.; Bouallou, C.; Couturier, K. Economic assessment of a power-to-substitute-natural-gas process including high-temperature steam electrolysis. *Int. J. Hydrogen Energy* **2015**, *40*, 6487–6500. [CrossRef]
33. Park, S.H.; Lee, Y.D.; Ahn, K.Y. Performance analysis of an SOFC/HCCI engine hybrid system: System simulation and thermo-economic comparison. *Int. J. Hydrogen Energy* **2014**, *39*, 1799–1810. [CrossRef]
34. Peters, M.S.; Timmerhaus, K.D.; West, R.E. *Plant Design and Economics for Chemical Engineers*, 5th ed.; McGraw-Hill Professional: New York, NY, USA, 2002.
35. Michailos, S.; McCord, S.; Sick, V.; Stokes, G.; Styring, P. Dimethyl ether synthesis via captured CO_2 hydrogenation within the power to liquids concept: A techno-economic assessment. *Energy Convers. Manag.* **2019**, *184*, 262–276. [CrossRef]
36. Wietschel, M. *Integration erneuerbarer Energien durch Sektorkopplung: Analyse zu technischen Sektorkopplungsoptionen*; Umweltbundesamt: Dessau-Roßlau, Germany, 2019.
37. Frontier Economics Strompreiseffekte eines Kohleausstiegs. 2018. Available online: https://www.frontier-economics.com/de/de/news-und-veroeffentlichungen/news/news-article-i4367-analysing-the-economic-impact-of-german-carbon-reduction-targets/ (accessed on 14 February 2023).
38. Winkler, J.; Sensfuß, F.; Pudlik, M. Leitstudie Strommarkt—Analyse ausgewählter Einflussfaktoren auf den Marktwert Erneuerbarer Energien. Karlsruhe, 2015. Available online: https://www.bmwk.de/Redaktion/DE/Publikationen/Studien/leitstudie-strommarkt_analyse-ausgewaehlter-einflussfaktoren-auf-den-martkwert-erneuerbarer-energien.html (accessed on 14 February 2023).
39. Kost, C.; Shammugam, S.; Fluri, V.; Peper, D.; Memar, A.D.; Schlegel, T. Levelized Cost of Electricity-Renewable Energy Technologies. Freiburg, 2021. Available online: https://www.ise.fraunhofer.de/en/publications/studies/cost-of-electricity.html (accessed on 14 February 2023).
40. Adnan, M.A.; Kibria, M.G. Comparative techno-economic and life-cycle assessment of power-to-methanol synthesis pathways. *Appl. Energy* **2020**, *278*, 115614. [CrossRef]
41. Battaglia, P.; Buffo, G.; Ferrero, D.; Santarelli, M.; Lanzini, A. Methanol synthesis through CO_2 capture and hydrogenation: Thermal integration, energy performance and techno-economic assessment. *J. CO_2 Util.* **2021**, *44*, 101407. [CrossRef]
42. Bellotti, D.; Rivarolo, M.; Magistri, L. Economic feasibility of methanol synthesis as a method for CO_2 reduction and energy storage. *Energy Procedia* **2019**, *158*, 4721–4728. [CrossRef]
43. Mohseni, E.; Herrmann-Heber, R.; Reinecke, S.F.; Hampel, U. Bubble generation by micro-orifices with application on activated sludge wastewater treatment. *Chem. Eng. Process. Process Intensif.* **2019**, *143*, 107511. [CrossRef]
44. Herrmann-Heber, R.; Reinecke, S.F.; Hampel, U. Dynamic aeration for improved oxygen mass transfer in the wastewater treatment process. *Chem. Eng. J.* **2020**, *386*, 122068. [CrossRef]
45. Gieseke, A.; Tarre, S.; Green, M.; de Beer, D. Nitrification in a biofilm at low pH values: Role of in situ microenvironments and acid tolerance. *Appl. Environ. Microbiol.* **2006**, *72*, 4283–4292. [CrossRef]
46. Fabiyi, M.; Connery, K.; Marx, R.; Burke, M.; Goel, R.; Snowling, S.; Schraa, O. Extending the Modeling of High Purity Oxygen Wastewater Treatment Processes: Transition from Closed to Open Basin Operations—A Full Scale Case Study. *Proc. Water Environ. Fed.* **2012**, *2012*, 4250–4262. [CrossRef]
47. DWA 31. *Leistungsnachweis Kommunaler Kläranlagen—Verfahren der Stickstoffelimination im Vergleich*; DWA: Hennef, Germany, 2018.

48. Institut für Wasserwirtschaft Halbach. Der biologische Sauerstoffbedarf im Ablauf von Kläranlagen. 7 August 2019. Available online: https://www.institut-halbach.de/2019/08/biologischer-sauerstoffbedarf-im-ablauf-von-klaeranlagen/ (accessed on 7 May 2023).
49. Larrea, A.; Rambor, A.; Fabiyi, M. Ten years of industrial and municipal membrane bioreactor (MBR) systems—Lessons from the field. *Water Sci. Technol.* **2014**, *70*, 279–288. [CrossRef]